Mechanical Analysis of Explanted Telescopic Rods in the Management of Osteogenesis Imperfecta: A Multicenter Study

NICOLAOU, Nicolas, LUO, Quanshun <http://orcid.org/0000-0003-4102-2129>, GILES, Stephen N., MARUTHAINAR, Kunalan, KITCHEN, Matthew P., THOMAS, Simon, FERNANDES, James A. and ROPOSCH, Andreas

Mechanical Analysis of Explanted Telescopic Rods in the Management of Osteogenesis Imperfecta- A Multi-Centre Study

Nicolaou N, Luo Q, Giles SN, Marathiar K, Kitchen M, Thomas S, Fernandes JA, Roposch A.

Nicolas Nicolaou *Bsc(*Hons) MBBS MRCS(Eng) MSc FRCS (Tr Orth), *Consultant Orthopaedic Surgeon, Sheffield Children's Hospital*

Quanshun Luo BSc MEng PhD Senior Research Fellow, *Sheffield Hallam University*

Stephen N. Giles MB BS, FRCS Ed(Tr Orth) *Consultant Orthopaedic Surgeon, Sheffield Children's Hospital*

Kunalan Marathiar MBBS, FRCS(Tr Orth) MD *Fellow, Great Ormond Street Hospital*

Matthew P. Kitchen *BEng(Hons) Researcher, Sheffield Hallam University*

Simon Thomas MA MBBS MRCS FRCS(Tr Orth) *Consultant Orthopaedic Surgeon, Bristol Royal Hospital for Children*

James A. Fernandes MBBS D Orth MS Orth Mch Orth DNB Orth FRCS (Tr Orth)

Consultant Orthopaedic Surgeon, Sheffield Children's Hospital

Andreas Roposch MD MSc FRCS(Tr Orth) *Professor of Surgery and Clinical Epidemiology Institute of Child Health, Consultant Paediatric Orthopaedic Surgeon Great Ormond Street Hospital*

Mechanical Analysis of Explanted Telescopic Rods in the Management of Osteogenesis Imperfecta- A Multi-Centre Study

Abstract

Background: Telescopic rods in the management of Osteogenesis Imperfecta (OI) fail frequently. This could be attributed to technical errors, rod design and rod structure. We aimed to analyse the mechanical properties and tribology of explanted male and female components to identify effects of *in vivo* telescoping by assessment of clinical, radiological, mechanical and tribological features.

Methods: Recruitment took place at 3 of the 4 English centres for OI. 25 rods explanted for growth or failure during revision to a new rod were analysed in terms of clinical indication and pre-revision imaging to identify if there was a technical mode of failure. Laboratory analysis was performed using optical and scanning electrical microscopy, radiograph diffraction analysis, hardness test, bending test and energy dispersive X-ray spectroscopy.

Results: All implants tested were of high grade stainless steel. Female components had inferior strength (mean Vickers hardness property ($HV_{0.3}$) at 0.3kg-313) in comparison to male components ($HV_{0.3}$ 406) due to different techniques of manufacture. Female rods also had a higher wear coefficient (7.89 □ 10^{-12} $m^3N^{-1}m^{-3}$) than the male rods (6.46 □ 10^{-12} $m^3N^{-1}m^{-3}$). Abrasive wear, shear deformation, scratches and wear debris were identified in all rods. Male and female components displayed biomedical deposits. Intra-operatively cut rods, particularly the female components, had irregular ends leading to more wear.

Conclusion: Current manufacturing techniques result in inferior material strength in female components compared to males, which combined with wear patterns is likely to lead to implant failure. Intra operative cutting of rods may increase risk of failure due to wear. Considering techniques to improve strength as well as design in new implants may lead to better outcomes.

Levels of Evidence: Level IV—cross-sectional study.

Key Words: osteogenesis imperfecta, metabolic bone disease, telescopic rodding

Introduction

Osteogenesis imperfecta (OI) is characterized by bone fragility (1,2). Deformity correction and prevention of recurrent fractures with telescopic intra-medullary rods benefits physical function and quality of life (3). The Bailey-Dubow rod (4), the first telescopic rod for OI, frequently failed because of T-piece detachment and migration (5,6). This problem was addressed by the next generation telescopic rods – the Sheffield rod (7) and the Fassier-Duval rod (8). These are made from a single steel section with provides more substantial fixation (9,10). However, intramedullary rods in patients with OI are still prone to fail with un-intended revision rates as high as 30-50% at mid-term follow up (10-13).

Un-intended revisions are often ascribed to technical errors with implantation (14) and severity of bone fragility (7). Patterns leading to un-intended revision include rod bending, disengagement following bone growth, and distal tibial and proximal femoral rod pull-out (7,15). We suggest that rod failure could also be attributed to the implant itself (e.g., design,

material). This study aimed to investigate the effects of implantation and *in vivo* telescoping on telescopic rods by assessment of clinical, radiological, mechanical and tribological features in retrieved implants; we further assessed if technical modes of failure during implantation produced different features of successful rod telescoping or failure.

Patients and Methods:

Following ethical approval, we performed a cross sectional study across 3 of the 4 Centres in England that manage complex Osteogenesis Imperfecta. 25 rods were selected as it would represent more than 4 cases of each common mode of failure (bending, fracture, pull-out distally, proximal sinking) and planned revisions for bone growth without rod failure. The latter would allow for comparison of any rod related factors that could be identified as different with failed rods and therefore characteristic of failure.

We included in this study any telescopic rod that was explanted from a skeletally immature tibia or femur in children with any type of OI. The 25 rods were from 18 patients.

Exclusion criteria were revision of non-telescopic rods, skeletal maturity at the time of rod insertion or an unconfirmed diagnosis of Osteogenesis Imperfecta. Basic demographic data was collected. Imaging of the affected bone was electronically linked without clinical information. Rods were explanted in a standardised fashion by all surgeons.

We conducted investigations blinded to study centre and patient characteristics. In order to exclude whether failure of rod was due to an implant error, we asked 4 experienced surgeons to rate the quality of rod implantation. The first post-operative full length anteroposterior and lateral radiographs of the tibia or femur after insertion were collected into a slide presentation at high resolution in random. Each surgeon, excluding the Chief Investigator, commented on the radiographs by grading each as having no, minor (unlikely to affect the telescoping) or major (likely to affect telescoping) technical errors. Each was asked to exclude any case they recognised as their own despite blinding. An error was considered if 2 or more of the 4 surgeons concurred (figure 1a & b).

Laboratory analysis

Each rod was macroscopically examined and photographed. Bending strength and hardness of the materials were measured. Analysis of tribological properties assessed surface wear and male/female rod interaction. Optical microscopy (OPM) and scanning electron microscopy (SEM) were performed for four sites of the male and female components with focus on the distal ends. For the female components, one end of each was ground to create an inclined flat end approximately 30□ to the axis expose the inner cylindrical surface. SEM analysis was performed on rods 1-11 and 15-25. The other rods were used for mechanical bending tests. Micro hardness tests were carried out to examine strength and the work-hardening behaviour of components. The hardness property was measured using a Mitutoyo HV/HK micro hardness tester. A Vickers' indenter was employed for indentation on pre-polished sample surfaces at a load of 0.3 kg. Hardness values were measured on specific longitudinal sections identified as identical on both longitudinal and transverse sections on the first 3 rods analysed.

A computer-controlled multi-functional tribometer (CERT-UMT-2) evaluated wear resistance. Male and female samples, cut as 20 mm long pieces, served as pin samples to slide in a reciprocating manner on a disc of resin-bonded Silicon Carbide (SiC). The wear coefficient was calculated as volume loss (cubic meter) at unit applied load (Newton) and unit sliding distance (metre), namely $m^3N^{-1}m^{-1}$. The wear properties were compared with other wear-resistant materials.

X-ray diffraction (XRD) analysis using Co-tube Empyrean X-ray diffractometry (PANalytical B.V., Netherlands) with cobalt radiation ($K_{\square}$-Co, □ = 0.1789 nm, powered at 40 kV and 40 mA) was used to study the manufacturing-related crystalline structural characteristics, indexed with respect to the presence of austenite phases.

Energy dispersive X-ray (EDX) spectroscopic analyses was performed to determine the elemental composition of polished samples and various as-received parts of the male and female components following electron microscopy to identify surface deposits.

Male and female components were evaluated in a standard three-point bending test using a universal tensile/bending/compression machine. Force-displacement curves were obtained. Using a formula (Appendix 1) the bending stresses at maximum and at yield were calculated. The bent sections of a subset of deformed rods had further hardness testing.

Results:

Mean age at implantation of the index rod was 5.44 years. Sixteen femoral segments and 9 tibial segments were treated. Time from insertion to revision was a mean 52.3 months (median 50.5). There were 20 Fassier-Duval (Pega Medical, Laval, Quebec, Canada) rods (9 tibial and 6 femoral) and 5 Sheffield (B. Braun Medial Ltd, UK) rods (all femoral). 20 of 25 were primary rodding procedures. Modes of failure are described in Table 1.

9 of the rods (36%) were considered to have minor technical errors unlikely to affect rod telescoping (Table 2). These errors were commonly related to minor mistakes in positioning, the commonest of which were related to entry points of the female component and distal location of the threads of the Fassier-Duval rods.

Laboratory Analysis

Macroscopic analysis revealed 14 of 25 rods had some degree of bending of the male and/or female components that was not always visible on pre-revision radiographs (Figure 2). The distal end of some female and male rods had irregularities (Figure 3).

The hardness values were similar within groups of male and female rods but were different by some margin between male and female components (Table 3). In every pair of telescopic rods, the male rod shows substantially higher hardness than the female rod. X-ray diffraction analysis identified that all the provided components could be classified as a grade of austenitic stainless steel AISI 316. Figure 4 shows an example of the XRD patterns of the rod and tube samples. In the two patterns, all the diffraction peaks fit well to the lattice planes of austenite. The lattice parameter has been estimated to be 0.3596 nm.

The males exhibit very fine microstructure and show fabric lines in the longitudinal sections. Such fabric features indicate a large scale of plastic deformation taking place in the

manufacturing process. Conversely the female rods exhibit coarse equiaxial microstructure both in the axial and longitudinal sections (Figure 5a and 5b). The coarse equaxial microstructure forms a big contrast to the extremely fine fabric microstructure, which suggests that the male and female rods were manufactured following different deforming processes. In particular, the female components experienced limited plastic deformation in manufacturing and consequently a lack of work-hardening. In addition, non-metallic inclusions of individual spherical particles of various sizes were observed on every section using optical microscopy.

The wear resistance of the male and female components differed with the female rod exhibiting higher wear coefficient (7.89×10^{-12} $m^3N^{-1}m^{-3}$) than the male (6.46×10^{-12} $m^3N^{-1}m^{-3}$) (Table 4). The wear coefficients of the telescopic male and female are in the same order. Under the applied abrasive test condition, the measured wear coefficients indicate the different resistance of the male and female rods to micro-cutting and to plastic deformation. The lower wear coefficient of the male rod was predominantly attributed to the higher hardness (Table 3).

Bending tests were carried out on three selected telescope rods (Nos 12, 13 and 14). The results are listed in Table 5. In addition, the hardness property measured from the bent areas is also listed in Table 5 to compare with the non-bent (original) areas, from which the increment in hardness indicates the magnitude of bending induced strain hardening. In the bending tests, the female components showed higher applied forces in the force-displacement curves, consistent with the larger size and tubular nature. However, the actual bending stresses in the females were substantially lower than the males and there was good correlation between the hardness measures and bending strength.

Further hardness testing was also performed on the 3-point bent sections of rods 13 and 14 to compare to the figures obtained for normal sections. The female rods show remarkably increased hardness in the bent areas as compared to the non-deformed (original) area. The increased hardness was attributed to the bending deformation because of the high straining hardening nature of austenitic stainless steel. In contrast, the male rods do not show significantly different hardness between the original and bent areas although the measured hardness values are substantially higher than the hardness of the female rods. The results suggest that the male rods had already been subjected to a large scale of cold-straining and subsequently been sufficiently work-hardened, so that the applied additional bending deformation did not lead to further hardening.

SEM

The results of SEM microstructure observation were consistent with the OPM observations.

Some straight scratches were located close to the distal end of the female. There were no such scratches proximally. This implies abrasive wear of the female caused by the male. These marks are deep and appear to result from sliding of the female against the male, which is believed to have risen from telescoping or during mating of the components at implantation. Visible shear deformation generating wear debris could be appreciated suggesting a twisting motion. Substantial small wear debris were seen at high magnification indicative of severe adhesive sliding contact between the male and female. The mechanisms

of wear identified include sliding-induced debris from micro-cutting; ploughing deformation, plastic fatigue wear due to repeated adhesive self-mating sliding contact (Figure 6).

The ends of females that had been cut intraoperatively were easily identified macroscopically (figure 3) by their irregular ends. On SEM these had rough burrs on the edges (Figure 7) that would have contributed to the tight sliding contact. Proportionate deformation was seen on the opposing male surface. Scratches were visible demonstrating abrasive wear, including plastic deformation grooves and fine wear debris either from micro-cutting or repeated plastic fatigue wear. Severe sliding grooves were apparent in the middle and distal male segments. The grooves in the central area were the most prominent. Those in the distal part were uniformly distributed over the surface. These features correspond to twisting and were probably caused by adhesive features during telescoping. The straight longitudinal sliding scratches seen in the male middle area also appear to occur with telescoping. In contrast, the male distal surface exhibits a uniform distribution of circular sliding grooves. These may occur intra-operatively, during mating of the components, or while screwing in the proximal female threads once the rods are engaged.

Using SEM-EDX analysis, the elemental compositions of the male and female were identical with typical elemental composition of austenitic stainless steel grade AISI 316. A deposit layer was found on the inner female surfaces. Details of the deposits are shown in Figure 8, including comparative energy X-ray spectroscopic analysis of the thick deposit, thin deposit and the fresh metallic surface (created by grinding prior to the SEM observation). The deposit is thick and becomes dispersive deposits in the places close to the distal female end. These deposits may be the result of biological corrosion (Figure 8). The male components also had contaminants on the surface (Figure 9). SEM-EDX analysis was applied on the contaminants and the contaminant-free inner surface (Figure 8 d-j, Table 6). SEM-EDX analysis of contaminant and contaminant-free inner surfaces showed the predominant presence of Iron, Chromium and Nickel in clean areas which are the major components of steel. In addition, it can be noticed that carbon and oxygen were detected in the freshly ground metallic steel surface. The presence of carbon and oxygen are unavoidable due to of condensed carbon during the vacuum pumping of the SEM chamber and the immediate surface oxidation of the Fe-Cr-Ni stainless steel in air. However, by comparing the EDX spectra of the deposits to the metallic area, we found that, in areas with surface contamination there were substantial amounts of carbonaceous material including carbon, oxygen and nitrogen, suggesting an organic origin. These may imply the presence of in-vivo corrosion although further more comprehensive analysis is required to verify such corrosion. The Sheffield components were not cut intra-operatively and had less wear debris and evidence of scratches.

When analysing the mode of failure, bearing in mind the variety of rods analysed no correlation could be identified with technical errors or mode of rod failure with wear patterns. Eight of the of nine rods that telescoped successfully and revised for growth were femoral rods with one tibial rod. These rods did not display any differences in terms of macroscopic irregularity of the female ends or different patterns of wear.

Discussion:

The telescopic rods in this study were all manufactured from high grade austenitic stainless steel with minimal impurities. There were nonetheless differences in rod strength between

male and female components with the latter less able to resist deformation on a material level because of the manufacturing process. The strong directional microstructure of the male results from the cold-forming manufacturing process. It may be that creating a female rod requires different processes for a suitable finish. Improved performance from alternative methods of manufacture may be possible (17-19).

Some wear and corrosion may be unavoidable with a telescopic rod design but intra-operative cutting of the Fassier-Duval components, especially the female, correlates with clear signs and specific modes of increased wear. Machine cutting of rods in the factory is likely to eradicate these features that were not seen with pre-cut Sheffield rods. There are additional costs to storing components of multiple sizes, especially in units without a high volume of cases, but this study strongly indicates a likely benefit to doing so. Additional wear occurred even in intra-operatively-cut implants that had telescoped successfully without bending. Furthermore, the biological corrosion between stainless steel implants and bodily fluids may be accelerated by additional wear particles (20-22).

Failures of telescopic rod are manifold and multifactorial in origin. Some factors, such as trauma, are unavoidable but technical aspects are also associated with failure (23). Undersized and/or malpositioned rods are less able to resist plastic deformation under load (24). Nonetheless the actual strength of the components to resist deformation and maintain telescoping are likely to be the predominant factors.

The appearance of bends within rods without trauma or technical error is intriguing (7,8,14,25). Rod insertion requires imposing straight anatomy on a long bone, in the case of the femur, that is naturally curved. Remodeling with growth may play a role in rod deformation and subsequent additional wear identified in this study.

Biological factors in failure are also possible. Organic films of varying thickness were identified on the components that are likely to increase resistance to telescoping and, ultimately, to contribute to pull out of the rods.

This study analyzed a limited but representative sample of rods of different designs and reasons for explantation. We accept that rod removal causes additional damage to the implants that might be misinterpreted as in vivo wear. All analyzed rods were explanted. Measurement of unused rods was not performed due to the prohibitive cost of these implants, and the focus of this study being the impact of implantation on the material properties. The tests performed on straight parts of the components could be slightly different to in an unused implant. Use of a 4-point bending test would have be superior in assessing material strength by allowing a longer period of maximum stress. Given material availability, we could only determine the bending property of the male, female, and male/female combination with the 3-point bending test. We were also not able to conduct any evaluation on stress shielding.

There are no previously published data on telescopic wear and analysis and so this series is a good benchmark for future studies. Future studies could look in more detail at rods that have failed in specific modes; for example, distal tibial pull-out that is common with threaded implants. We could find no clear correlation between modes of failure and different patterns of wear. Although the rod:canal ratio at the narrowest point of the diaphysis for both femur and tibia were measured, these data were excluded. Owing to the nature of severe OI, the complexity of the deformity can often limit rod size, and standard radiograph projections are likely to miss such deformity which is best assessed with 3-

dimensional imaging. Such information would be useful as the ideal rod size is likely to have bearing on rod failure.

Numerous rod designs have been developed to improve implant fixation and maintain telescoping (26–29). The mode of proximal and distal fixation is often thought to be the reason for rod failure. Rod choice is based on training and clinical preference, with the Fassier-Duval most popular due to the ability to insert this rod from just the proximal part of the long bone. This study also included the Sheffield rod which requires access both proximally and distally due to the presence of T-piece fixation, but we have not compared the rod methods of wear due to small representative samples, and the analysis of wear is not aimed at comparing the different implants. Data on revision already exists to allow users of these systems to make an informed choice on which performs better clinically.

In conclusion, this study has confirmed the inferior mechanical strength property of female rods to be the main cause of bending failure. This study also has identified patterns of wear and possible corrosion that would support the use of machine pre-cut implants despite the additional costs. Manufacturing techniques should be re-evaluated with a view to achieving the same strength and surface quality of the male components for the female components. This is perhaps as, if not more important than the method of proximal and distal rod fixation.

References:

1. Folkestad L, Hald JD, Ersbøll AK, et al. Fracture Rates and Fracture Sites in Patients with Osteogenesis Imperfecta: A Nationwide Register-Based Cohort Study. *J Bone Miner Res*. 2017;32(1):125-134.
2. Peddada KV, Sullivan BT, Margalit A, Sponseller PD. Fracture Patterns Differ Between Osteogenesis Imperfecta and Routine Pediatric Fractures. *J Pediatr Orthop*. 2018;38(4
3. Ruck J, Dahan-Oliel N, Montpetit K, Rauch F, Fassier F. Fassier-Duval femoral rodding in children with osteogenesis imperfecta receiving bisphosphonates: functional outcomes at one year. *J Child Orthop*. 2011;5(3):217-224
4. Marafioti RL, Westin GW. Elongating intramedullary rods in the treatment of osteogenesis imperfecta. *J Bone Joint Surg Am*. 1977;59(4):467-472.
5. Gamble JG, Strudwick WJ, Rinsky LA, Bleck EE. Complications of intramedullary rods in osteogenesis imperfecta: Bailey-Dubow rods versus nonelongating rods. *J Pediatr Orthop*. 1988;8(6):645-649.
6. Lang-Stevenson AI, Sharrard WJ. Intramedullary rodding with Bailey-Dubow extensible rods in osteogenesis imperfecta. An interim report of results and complications. *J Bone Joint Surg Br*. 1984;66(2):227-232.
7. Nicolaou N, Bowe JD, Wilkinson JM, Fernandes JA, Bell MJ. Use of the Sheffield telescopic intramedullary rod system for the management of osteogenesis imperfecta: clinical outcomes at an average follow-up of nineteen years. *J Bone Joint Surg Am*. 2011;93(21):1994-2000.

8. Azzam KA, Rush ET, Burke BR, Nabower AM, Esposito PW. Mid-term Results of Femoral and Tibial Osteotomies and Fassier-Duval Nailing in Children with Osteogenesis Imperfecta. *J Pediatr Orthop*. 2018;38(6):331-336.
9. Stockley I, Bell MJ, Sharrard WJ. The role of expanding intramedullary rods in osteogenesis imperfecta. *J Bone Joint Surg Br*. 1989;71(3):422-427.
10. Mulpuri K, Joseph B. Intramedullary rodding in osteogenesis imperfecta. *J Pediatr Orthop*. 2000;20(2):267-273.
11. Spahn KM, Mickel T, Carry PM, et al. Fassier-Duval Rods are Associated with Superior Probability of Survival Compared With Static Implants in a Cohort of Children With Osteogenesis Imperfecta Deformities. *J Pediatr Orthop*. 2019;39(5):e392-e396.
12. Scollan JP, Jauregui JJ, Jacobsen CM, Abzug JM. The Outcomes of Nonelongating Intramedullary Fixation of the Lower Extremity for Pediatric Osteogenesis Imperfecta Patients: A Meta-analysis. *J Pediatr Orthop*. 2017;37(5):e313-e316.
13. Joseph B, Rebello G, B CK. The choice of intramedullary devices for the femur and the tibia in osteogenesis imperfecta. *J Pediatr Orthop B*. 2005;14(5):311-319.
14. Lee RJ, Paloski MD, Sponseller PD, Leet AI. Bent Telescopic Rods in Patients with Osteogenesis Imperfecta. *J Pediatr Orthop*. 2016;36(6):656-660.
15. Cox I, Al Mouazzen L, Bleibleh S, et al. Combined two-centre experience of single-entry telescopic rods identifies characteristic modes of failure. *Bone Joint J*. 2020;102-B(8):1048-1055. doi:10.1302/0301-620X.102B8.BJJ-2020-0131.R1
16. Warman ML, Cormier-Daire V, Hall C, et al. Nosology and classification of genetic skeletal disorders: 2010 revision. *Am J Med Genet A*. 2011;155A(5):943-968.
17. Muley SV, Vidvans AN, Chaudhari GP, Udainiya S. An assessment of ultra fine grained 316L stainless steel for implant applications. *Acta Biomater*. 2016;30:408-419.
18. Asri RIM, Harun WSW, Samykano M, et al. Corrosion and surface modification on biocompatible metals: A review. *Mater Sci Eng C Mater Biol Appl*. 2017;77:1261-1274.
19. Bekmurzayeva A, Duncanson WJ, Azevedo HS, Kanayeva D. Surface modification of stainless steel for biomedical applications: Revisiting a century-old material. *Mater Sci Eng C Mater Biol Appl*. 2018;93:1073-1089.
20. Liu Y, Zhu D, Pierre D, Gilbert JL. Fretting initiated crevice corrosion of 316LVM stainless steel in physiological phosphate buffered saline: Potential and cycles to initiation. *Acta Biomater*. 2019;97:565-577.
21. Tiamiyu AA, Eduok U, Szpunar JA, Odeshi AG. Corrosion behavior of metastable AISI 321 austenitic stainless steel: Investigating the effect of grain size and prior plastic deformation on its degradation pattern in saline media. *Sci Rep*. 2019;9(1):12116. Published 2019 Aug 20.
22. Xu W, Yu F, Yang L, Zhang B, Hou B, Li Y. Accelerated corrosion of 316L stainless steel in simulated body fluids in the presence of H_2O_2 and albumin. *Mater Sci Eng C Mater Biol Appl*. 2018;92:11-19.

23. Holmes K, Gralla J, Brazell C, et al. Fassier-Duval Rod Failure: Is it Related to Positioning in the Distal Epiphysis? [published online ahead of print, 2020 Feb 6]. *J Pediatr Orthop*. 2020.

24. Lee K, Park MS, Yoo WJ, Chung CY, Choi IH, Cho TJ. Proximal migration of femoral telescopic rod in children with osteogenesis imperfecta. *J Pediatr Orthop*. 2015;35(2):178-184.

25. Nicholas RW, James P. Telescoping intramedullary stabilization of the lower extremities for severe osteogenesis imperfecta. *J Pediatr Orthop*. 1990;10(2):219-223.

26. Rosemberg DL, Goiano EO, Akkari M, Santili C. Effects of a telescopic intramedullary rod for treating patients with osteogenesis imperfecta of the femur. *J Child Orthop*. 2018;12(1):97-103.

27. Shin CH, Lee DJ, Yoo WJ, Choi IH, Cho TJ. Dual Interlocking Telescopic Rod Provides Effective Tibial Stabilization in Children with Osteogenesis Imperfecta. *Clin Orthop Relat Res*. 2018;476(11):2238-2246.

28. Cho TJ, Choi IH, Chung CY, Yoo WJ, Lee KS, Lee DY. Interlocking telescopic rod for patients with osteogenesis imperfecta. *J Bone Joint Surg Am*. 2007;89(5):1028-1035.

29. Cho TJ, Kim JB, Lee JW, et al. Fracture in long bones stabilised by telescopic intramedullary rods in patients with osteogenesis imperfecta. *J Bone Joint Surg Br*. 2011;93(5):634-638.

Legends:

Figure 1a and b: Rod 17- AP and Lateral view. Type IV OI with previous multiple fractures managed with Fassier-Duval Rod for diaphyseal fracture of the right tibia. Described as technically adequate by all reviewing surgeons. Revised at 21 months for a mobile female component blocking knee extension.

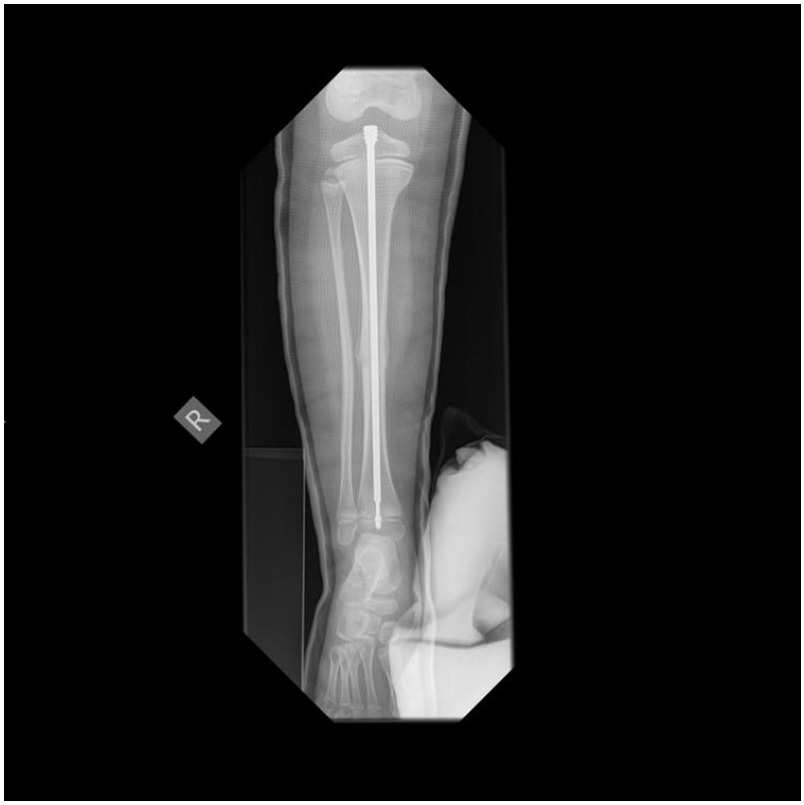

Figure 2: Photograph of rod samples 6 to 10. The red line is used to reference deviation from straight in the plane of maximal bow. Red arrows identify the apex of deformity.

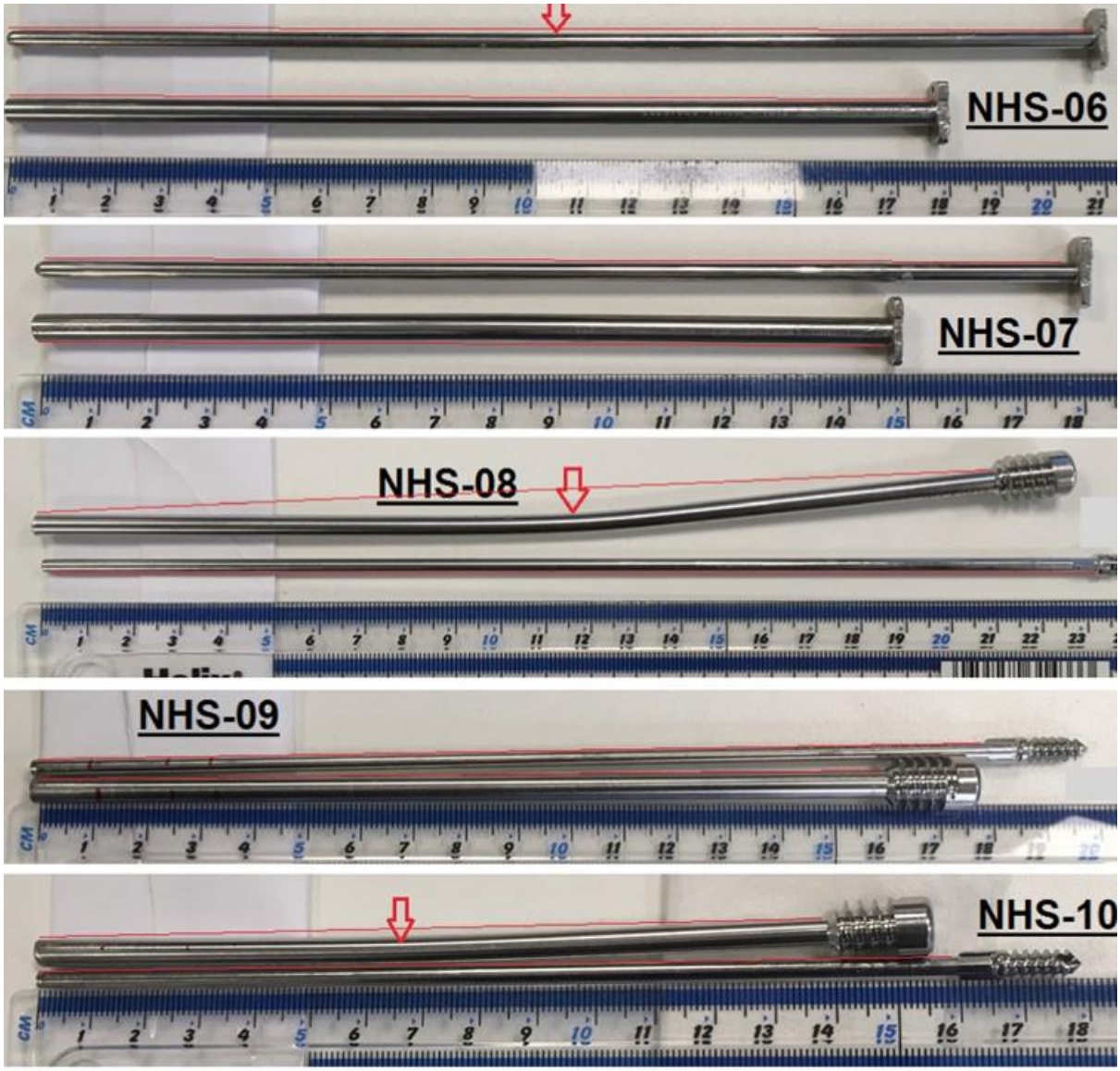

Figure 3: Photograph of the distal female and proximal male of rods 6 and 7 (Sheffield rods) and 8-11 (Fassier-Duval). Variability in the cut rod ends can be seen.

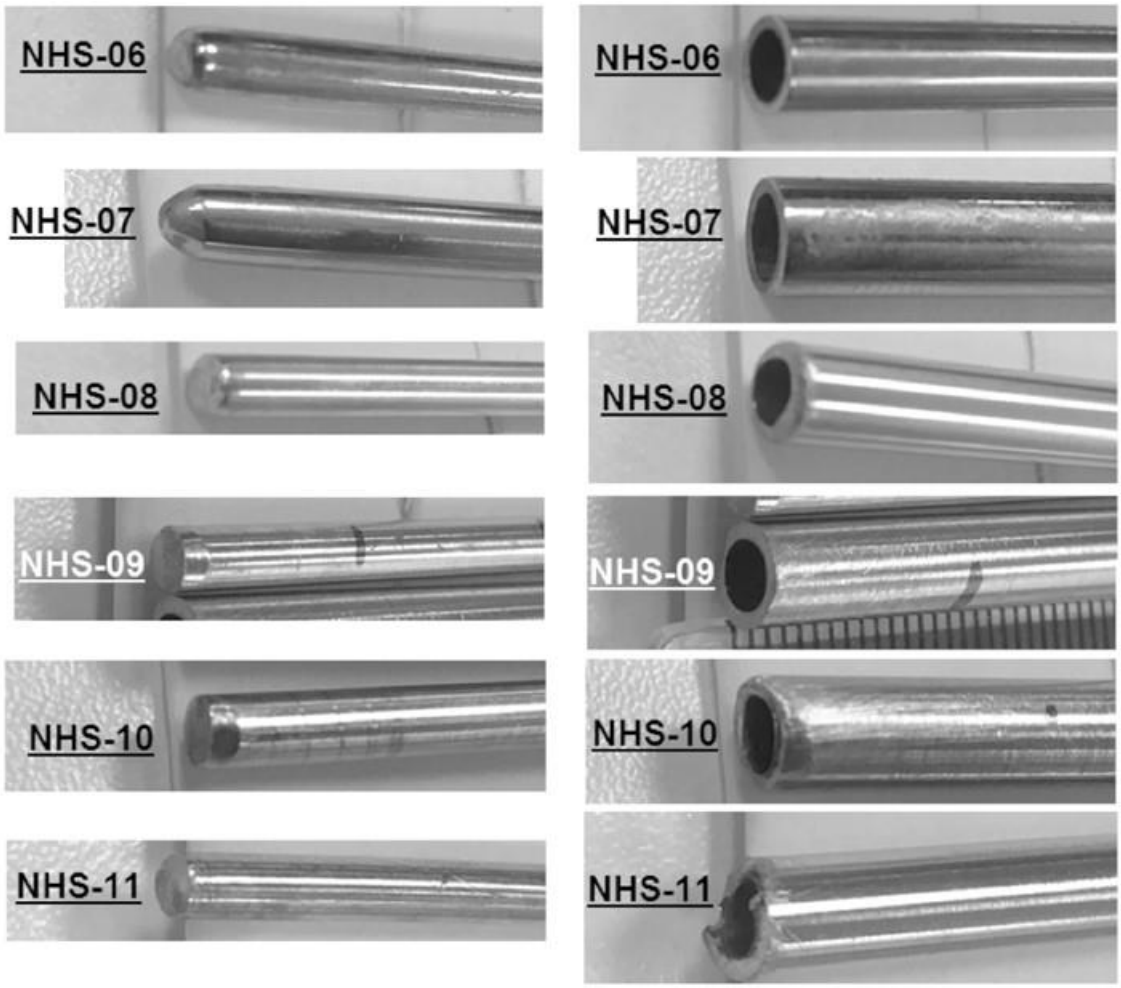

Figure 4 X-diffraction patterns of (a) the Rod and (b) the Tube samples. Note that the diffraction peaks all fit to the face-centre-cubic austenite crystalline phase of austenitic stainless steel.

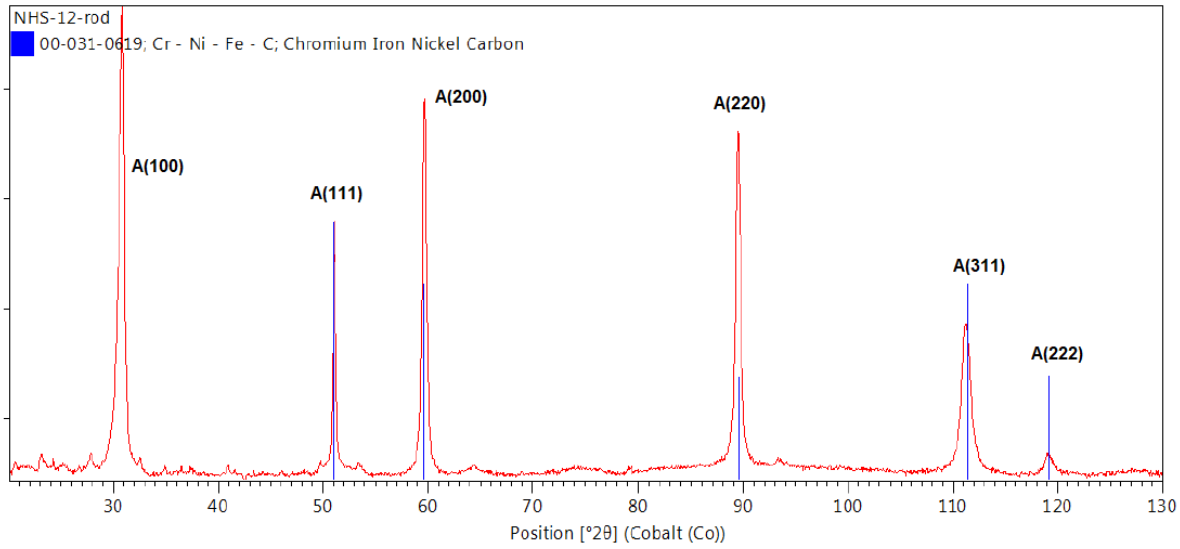

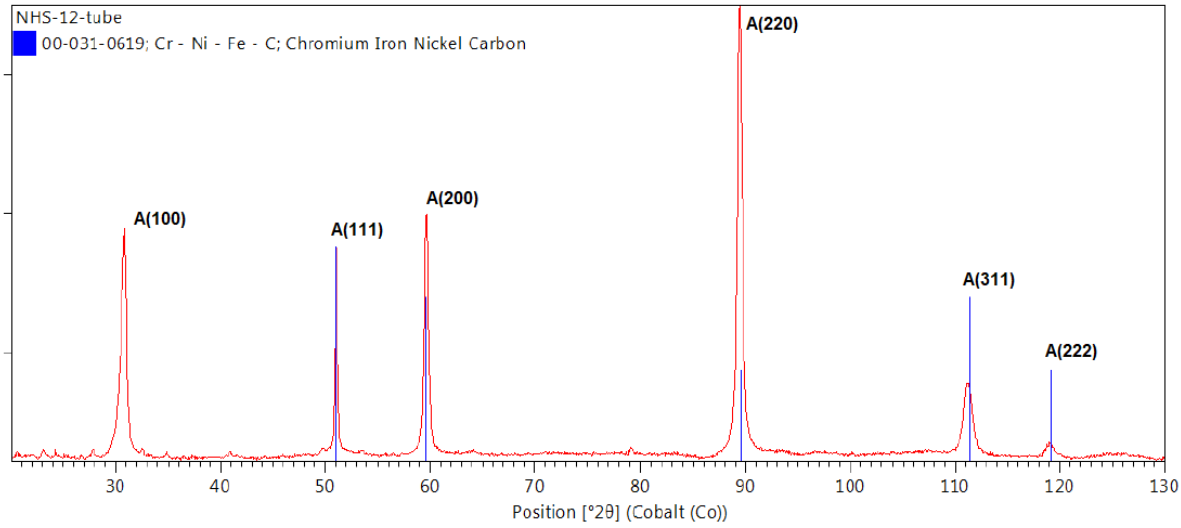

Figure 5: Optical microstructure of rod 3 Male (a) and Female (b) identifying differences in the coarse axial microstructure.

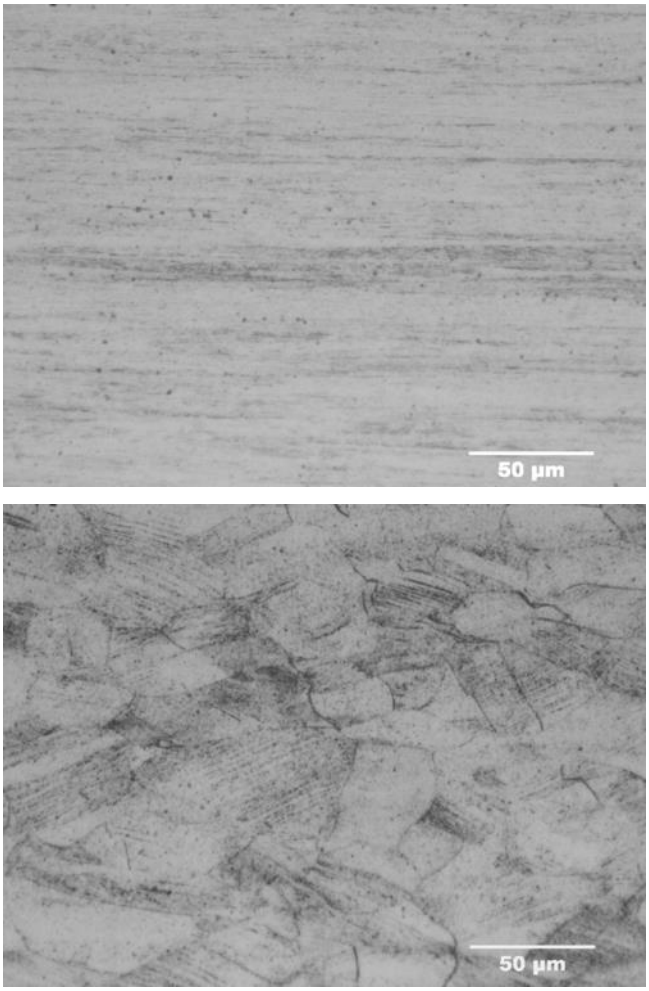

Figure 6: Photomicrograph of inner surface of female rod 1 distal end. The rough surface finish with loose fragments can be seen (inset photo at higher magnification). Region III is the end of deforming manufacture of the inner cylindrical surface, and region IV shows severe grooving deformation and attached debris.

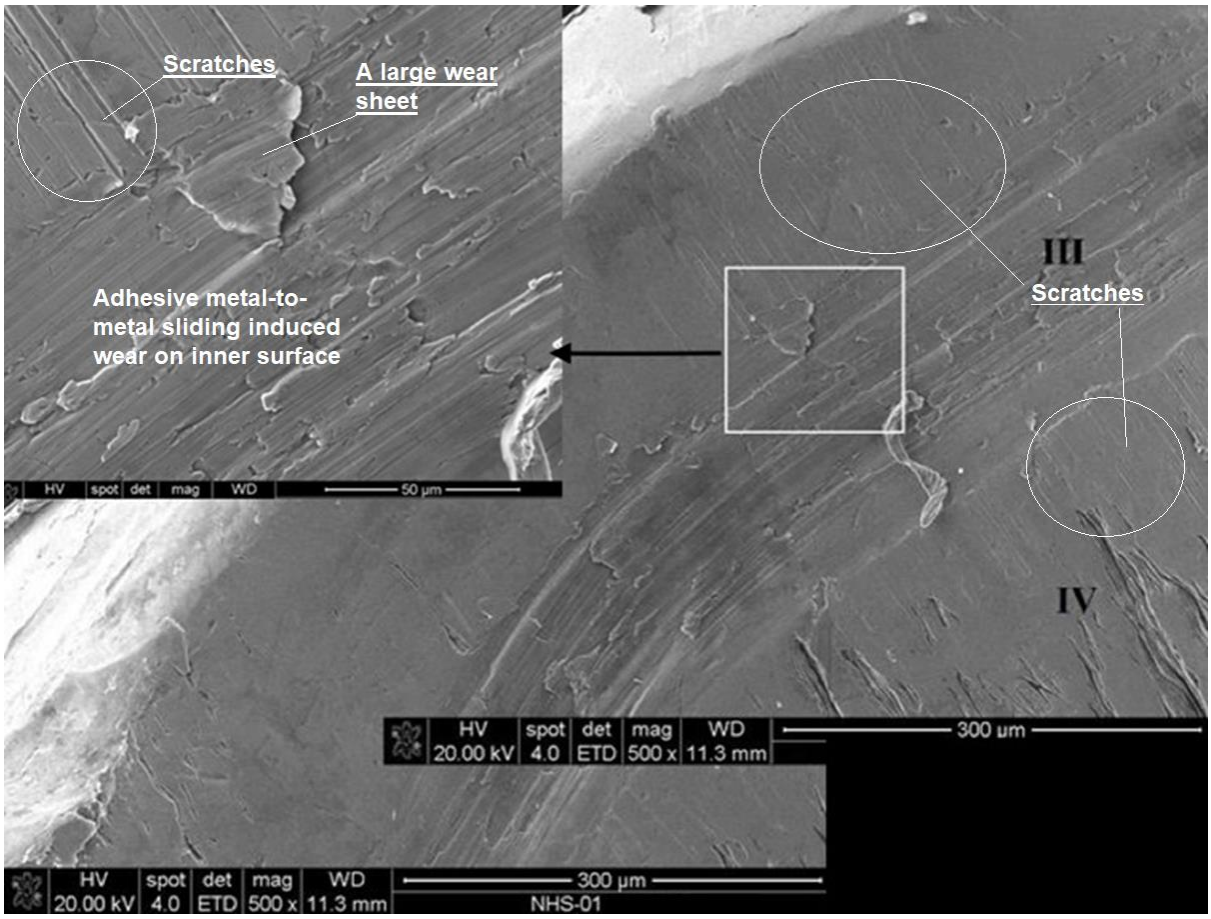

Figure 7: Photomicrograph of inner surface of female rod 10 showing irregularity of the cut ends, inset photomicrograph at higher magnification.

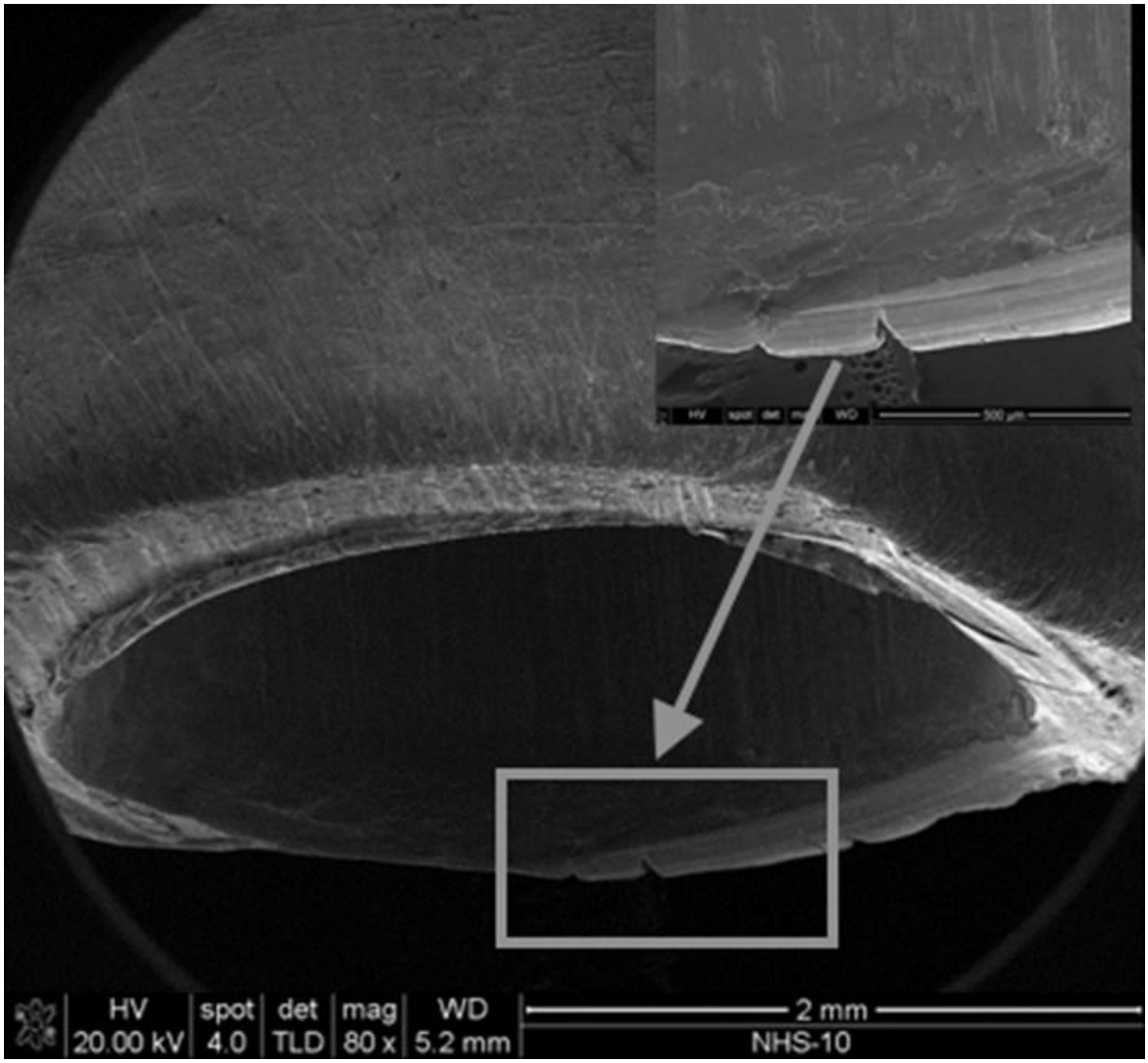

Figure 8: SEM observations of the inner surface of a female rod at various magnifications (a-c) and associated energy dispersive X-ray spectroscopic analysis of the metallic surface (d, h), thick deposit (e, i) and thin deposit (g, j).

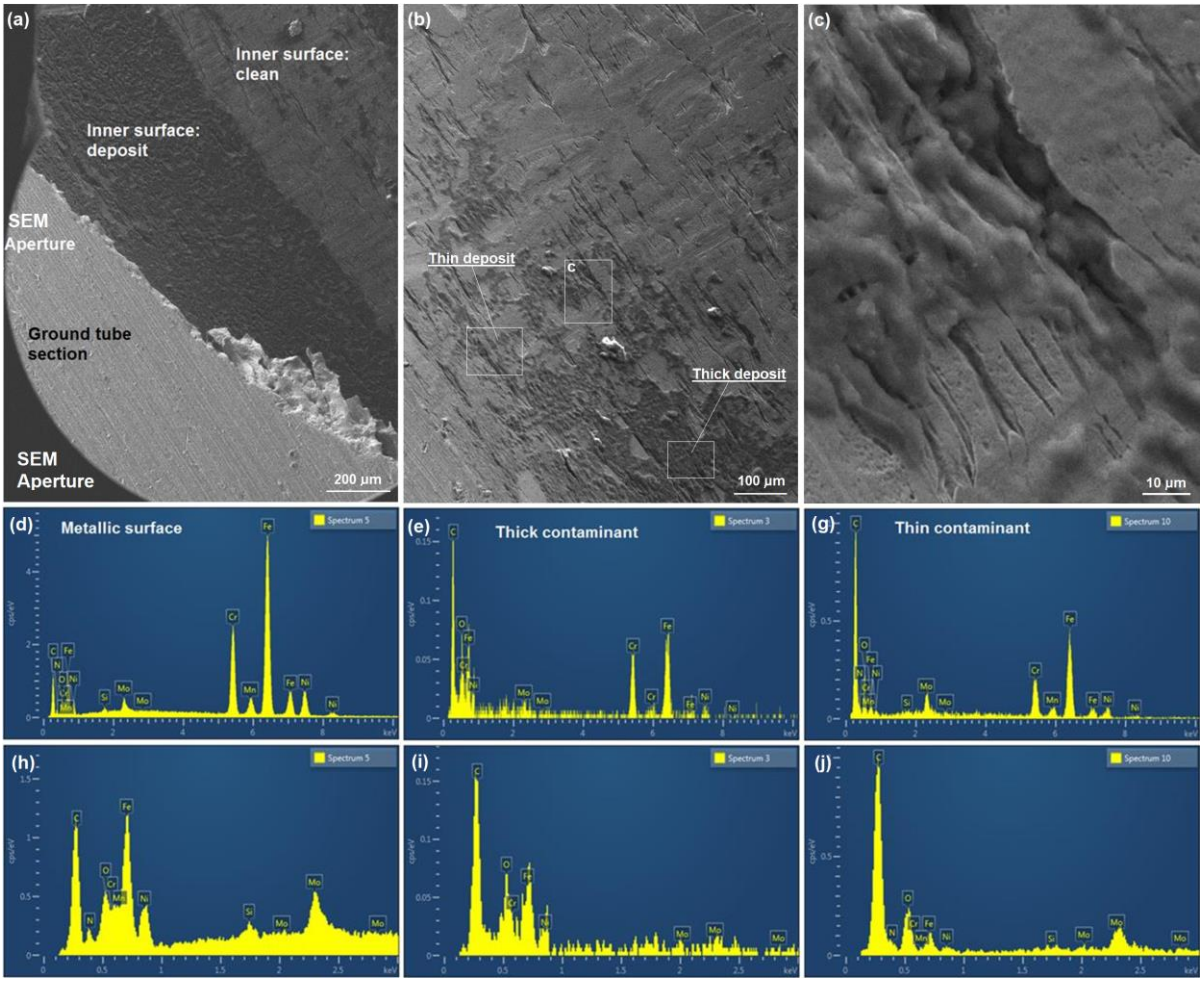

Figure 9: Biochemical deposits on the distal end of male rod 1 at low and high magnification.

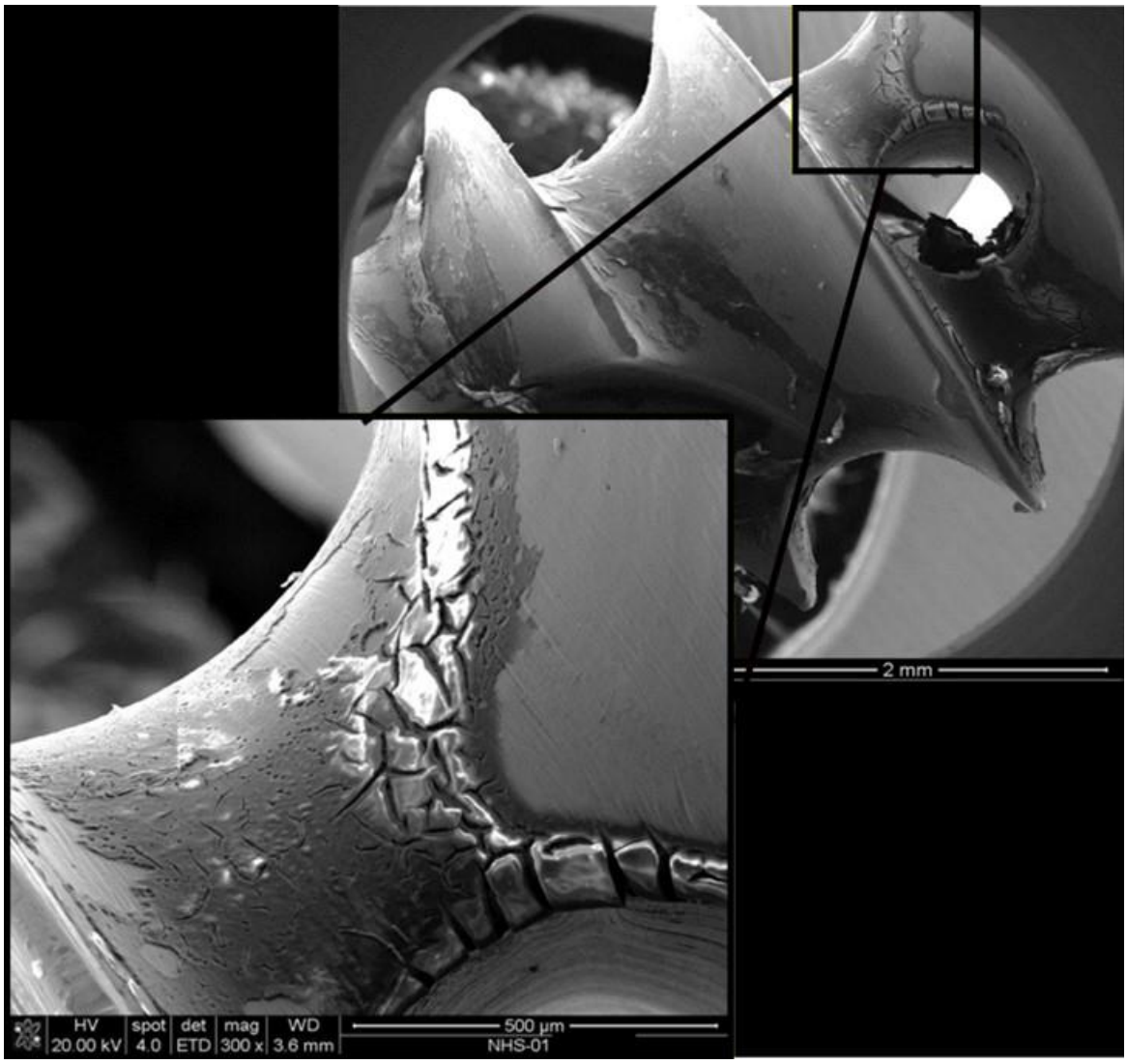

Table 1 Demographics of the Analyzed Rods

STUDY NO.	OI TYPE	SEG MENT	ROD ANALYSED	REVISED FROM	OSTEO TOMIES	INDICATION FOR REVISION	REVISED TO
1	III	R TIBIA	FD	SHEFFIELD SINGLE	1	DEFORMITY, DISTAL CUT OUT ANTERIORLY	FD
2	III	L TIBIA	FD	SHEFFIELD SINGLE	1	DEFORMITY, DISTAL CUT OUT ANTERIORLY	FD
3	IV	L FEMUR	SHEFFIELD	SHEFFIELD ROD	0	BENT ROD COXA VARA	SHEFFIELD
4	IV	R FEMUR	SHEFFIELD	NO ROD	2	GROWTH	LOCKED NAIL
5	I	L FEMUR	SHEFFIELD	NO ROD	1	GROWTH	SHEFFIELD
6	IV	L FEMUR	SHEFFIELD	SHEFFIELD ROD	1	GROWTH	SHEFFIELD
7	IV	R FEMUR	SHEFFIELD	SHEFFIELD ROD	0	GROWTH	SHEFFIELD
8	IV	L FEMUR	FD	FD	2	DISTAL PULL OUT EPIPHYSIS	FD
9	III	R FEMUR	FD	RUSH ROD	1	PROX PULL OUT	FD
10	III	R FEMUR	FD	FD	0	DISTAL PULL OUT, PROX FRACTURE AND BENT ROD	FD
11	I	L FEMUR	FD	RUSH ROD	2	GROWTH	FD
12	V	L FEMUR	FD	RUSH ROD	2	DISTAL PULL OUT EPIPHYSIS, BENT ROD	FD
13	III	R TIBIA	FD	NO ROD	1	DEFORMITY BENT ROD	FD
14	III	L FEMUR	FD	FD	1	DEFORMITY BENT ROD	SHEFFIELD
15	III	R FEMUR	FD	NO ROD	1	FRACTURE, BENT ROD	FD
16	III	L TIBIA	FD	FD	0	FRACTURE, BENT ROD	FD
17	IV	R TIBIA	FD	NO ROD	0	LOOSE FEMALE AT KNEE BLOCKING EXTENSION	TST
18	III	L TIBIA	FD	FD	1	DEORMITY AND FRACTURE	TST
19	III	R TIBIA	FD	FD	1	PERSISTENT DEFORMITY	TST
20	III	R FEMUR	FD	RUSH ROD	1	GROWTH	FD
21	III	L TIBIA	FD	RUSH ROD	1	FRACTURE, BENT ROD	FD
22	III	L FEMUR	FD	RUSH ROD	1	GROWTH	FD
23	III	R TIBIA	FD	RUSH ROD	2	GROWTH	FD
24	III	R FEMUR	FD	FD	0	PROX MIGRATION AND GROWTH	FD
25	III	L FEMUR	FD	RUSH ROD	1	GROWTH	FD

Table 2 All Technical Errors Identified for Each Analyzed Rod

Tibial rod	**Femoral Rod**
female entry too anterior (3)	undersized rod (3)
male too long (3)	lateral entry (3)
medial entry (2)	female too long impacting on male flutes (2)
eccentric positioning of female	male too far in (2)
male threads too short	medial entry (2)
required further osteotomy	varus proximal femur above osteotomy (2)
rod slight bend	male threads fixed posterior
undersized rod	male threads undersized
	female left proud proximally

Table 3 Hardness Values of Rod 1 to 14

	ROD 1	ROD 2	ROD 3	ROD 4	ROD 5	ROD 6	ROD 7	ROD 8
ROD TYPE	FD	FD	SHEFFIELD	SHEFFIELD	SHEFFIELD	SHEFFIELD	SHEFFIELD	FD
MALE	395	402	448	460	439	419	424	390
FEMALE	317	331	302	313	357	292	311	314

	ROD 9	ROD 10	ROD 11	ROD 12	ROD 13	ROD 14		MEAN
ROD TYPE	FD	FD	FD	FD	FD	FD		
MALE	375	374	362	362	432	408		**406**
FEMALE	257	305	294	330	336	318		**313**

Table 4 Wear Coefficient (k) for the Male and Female Components of Rod 5

Sample	**Sliding**	**Mass loss**	**Volume loss***	**K**	**Friction**
ROD 5 FEMALE	**m**	**mg**	**mm^3**	**10^{-12} $m^3N^{-1}m^{-1}$**	
1	0	0	0		
2	11.4	1.6	0.21	9.18	0.70
3	11.4	1.3	0.17	7.46	0.69
4	11.4	1.4	0.18	8.03	0.67
5	11.4	1.2	0.15	6.89	0.63
			Average	**7.89**	**0.67**
ROD 5 MALE					
1	0	0	0	0	
2	11.4	1.6	0.21	9.18	0.82
3	11.4	0.6	0.08	3.44	0.65
4	11.4	0.9	0.12	5.16	0.61
5	11.4	1.4	0.18	8.03	0.82
			Average	**6.46**	**0.73**

Table 5 The Bending Strength Property and Bending Induced Work-Hardening of Selected Rods

	Bending strength [MPa]			Hardness (male)		Hardness (female)	
	Male	Female	Combined	Original	Bent	Original	Bent
Rod 12	1100	637	987	362		330	
Rod 13	986	946	1258	432	412	336	363
Rod 14	1100	689	882	408	410	318	354

Table 6 Elemental Compositions (in Weight%) of the Contaminant on the Inner Tube Surface of Rod 1

	C	**O**	**Cr**	**Ni**	**Mo**	**Fe**	**Area**
EDX-4	33.3	4.8	13.6	6.8	1.3	38.9	Metal surface
EDX-5	24.7	3.1	13.2	9.0	2.1	42.3	Metal surface
EDX-6	22.5	3.0	14.5	9.5	2.0	46.5	Metal surface
EDX-3	54.7	14.6	9.3	3.0	1.3	17.0	Thick contaminant
EDX-7	57.0	13.5	7.2	3.2	3.3	15.6	Thick contaminant
EDX-8	53.1	16.0	7.1	3.6	1.1	17.9	Thick contaminant
EDX-9	46.1	4.5	9.5	5.3	3.3	30.5	Thin contaminant
EDX-10	49.9	13.5	4.6	2.6	2.5	14.0	Thin contaminant